Journal of Mechatronics, Electrical Power, and Vehicular Technology 10 (2019) 17–23

Journal of Mechatronics, Electrical Power, and Vehicular Technology

e-ISSN: 2088-6985
p-ISSN: 2087-3379

www.mevjournal.com

Load characteristic analysis of a double-side internal coreless stator axial flux PMG

Ketut Wirtayasa [a, b, *], Pudji Irasari [a], Muhammad Kasim [a, c], Puji Widiyanto [a], Muhammad Fathul Hikmawan [a]

[a] *Research Centre for Electrical Power and Mechatronics, Indonesian Institute of Sciences*
Jl. Cisitu No. 154D, Bandung, 40135, Indonesia

[b] *Department of Electrical Engineering, National Taiwan University of Science and Technology,*
No. 43, Section 4, Keelung Rd, Da'an District, Taipei City, 106, Taiwan

[c] *School of Electrical Engineering and Telecommunications, University of New South Wales*
330 Anzac Parade, Kensington NSW 2033, Australia

Received 15 March 2019; accepted 29 November; Published online 17 December 2019

Abstract

The main issue of using a permanent magnet in electric machines is the presence of cogging torque. Several methods have been introduced to eliminate it, one of which is by employing a coreless stator. In this paper, the load characteristic analysis of the double-side internal coreless stator axial flux permanent magnet generator with the specification of 1 kW, 220 V, 50 Hz, 300 rpm and 1 phase is discussed. The purpose is to learn the effect of the load to the generator performance, particularly the output power, efficiency and voltage regulation. The design and analysis are conducted analytically and numerically with two types of simulated loads, pure resistive and resistive-inductive in series. Each type of load provides power factor 1 and 0.85 respectively. The simulation results show that when loaded with resistive load, the generator gives a better performance at the output power (1,241 W) and efficiency (91 %), whereas a better voltage regulator (5.86 %) is achieved when it is loaded with impedance. Since the difference in the value of each parameter being compared is relatively small, it can be concluded that the generator represents good performance in both loads.

Keywords: coreless stator; axial flux permanent magnet generator; load characteristics; resistive load; resistive-inductive in series.

I. Introduction

Axial-flux permanent magnet generators (AFPMG) offer several benefits, among others, can be made in various alternative topologies [1] and have high power density [2][3]. Their application is not only in the electricity generation sector but also in electric vehicles, industrial equipment [4], aircraft, compact engine generator, and battery charging [5].

The stator of AFPMG can be built with or without iron core. The latter gives some more advantages since it is lighter than the construction of using core, eliminates cogging torque, easy to manufacture, because it does not need lamination and eliminates magnetic forces to the rotor disc [6] as well as having high efficiency [5][7]. Several types of research on the AFPM coreless stator have been conducted and most of them are used in wind turbine applications. Reference [6] analyzes a double-sided coreless-stator 24 poles and 18 coils AFPMG. The best generator performance can be obtained by varying stator thickness and diameter. The highest efficiency is 91.8 % acquired from the combination of the stator thickness and diameter of 8 mm and 150 mm.

Design and analysis of three rotors and double stators coreless AFPMG are observed in [8]. By configuring 12 poles in each rotor and 9 coils in each stator, the generator can produce 1.8 kW and 120 V at 500 rpm. Three rotors are used instead of 4 so that reducing the iron loss and the generator weight. A similar pole configuration is found in [9], which is 12 permanent magnet at each of the rotor core (double rotors) and 9 coils in the stator (single stator). The simulation results indicate that the 500 rpm coreless AFPMG can generate nearly sinusoidal voltage and

* Corresponding Author. Tel: +62-81223114327
E-mail address: ktwirtayasa@yahoo.co.id

doi: https://dx.doi.org/10.14203/j.mev.2019.v10.17-23

Accreditation Number: (LIPI) 633/AU/P2MI-LIPI/03/2015 and (RISTEKDIKTI) 1/E/KPT/2015.

current waveforms. The amplitude of the waveforms is 100 V and 5 A respectively. In reference [10], design and prototyping of 3 phase, coreless AFPMG with two rotors and one stator is investigated. The configuration of 20 poles on the rotors and 18 coils on the stator is employed. The measurement test at 300 rpm yields terminal voltage, output power, and efficiency, respectively are 200 V, 200 W, and 94.2 %.

The paper discussed the load characteristics of a 220 V, 1 kW, 50 Hz, 300 rpm 1 phase coreless axial flux generator. The simulation is conducted analytically and numerically by employing pure resistive load as well as resistive-inductive loads in series. The aim of this research is studying the effect of the load, mainly on the generator output power, efficiency, and voltage regulation. In addition to the load characteristics, the magnetic flux distribution and air gap flux density simulated using FEMM 4.2 software will also be presented.

II. Materials and Methods

A. The design feature of the machine

The generator topology, dimensions, and main parameters are illustrated in Figure 1 and Table 1 respectively. The rotor is the rotating part of a generator where the permanent magnets are arranged on the inside (Fig. 1a). The stator is the stationary part and the place for the winding (Fig. 1b). The stator and rotor are integrated through a shaft to produce electricity. The constructions of the studied double rotor single coreless stator, as well as its dimensions in the axial direction, are shown in Fig. 1c and Fig. 1d respectively.

Table 1.
The dimension of the generator parts

Parameter	Unit
Outer rotor disc radius, Rro	200 (mm)
Inner rotor disc radius, Rri	115 (mm)
Winding thickness, t_w	4 (mm)
Rotor yoke thickness, Ly	60 (mm)
Number of turns, N_1	340 turn
Number of poles, 2P	20 poles
Number of parallel conductor, a_w	2
Wire diameter, dw	0.8 (mm)
Shaft radius, Rsh	30 (mm)
Permanent magnet axial height, h_m	40 (mm)
Inner permanent magnet arc, Wpi	28.9 (mm)
Outer permanent magnet arc, Wpo	50.27 (mm)
Permanent magnet length, Lp	85 (mm)
Air gap length, l_g	3 (mm)

B. The magnetic field in coreless AFPMG

The flux paths of the double-sided rotors internal coreless stator AFPMG is depicted in Fig. 2. The stator is made without core (coreless) and the rotor is made of carbon steel. The flux leave north pole (permanent magnet 1) across stator and air gap to the south pole (permanent magnet 2) and then splits into two equal sections, one of them travels toward south poles of permanent magnet 3, and then passing through the stator as well as air gap to the south pole of permanent magnet 4, as shown by arrow signs.

NdFeB has been used as the permanent magnet with Br = 1.030 T and the coercive field strength Hc = 796 kA/m. moreover, Air gap flux density (B_{mg}) and magnetic flux (ϕ_f) are stated at equation (1) and equation (2) [11][12],

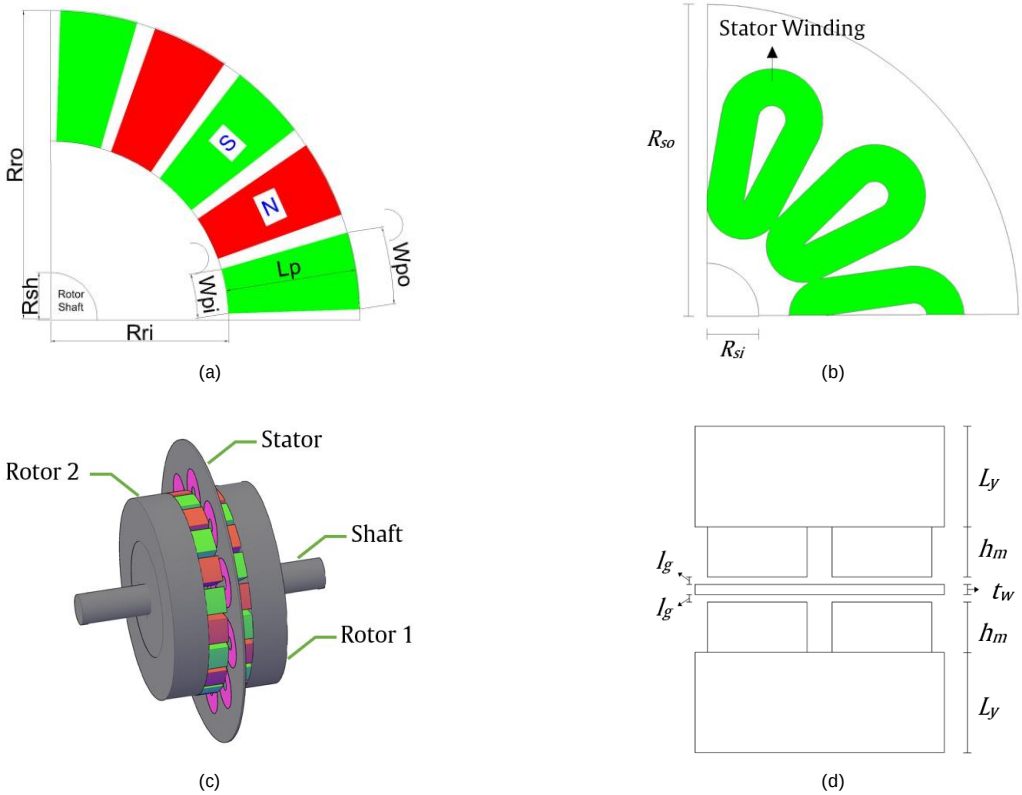

Figure 1. Generator dimensions; (a) rotor; (b) stator and its winding configuration; (c) three dimensional coreless AFPMG; (d) front view

$$\boldsymbol{B_{mg}} = \frac{\boldsymbol{B_r}}{\mathbf{1}+[\frac{\mu_{rrec}(g+0.5t_w)}{h_m}]\boldsymbol{k_{sat}}} \quad (1)$$

$$\phi_f = \alpha_i B_{mg} \frac{\pi}{8p}(D_{ro}^2 - D_{ri}^2) \quad (2)$$

where B_r is the remanence flux (T), μ_{rrec} is the relative permeability of permanent magnet, g is the axial length of the air gap (mm), t_w is the winding thickness (mm), h_m is the axial height of the permanent magnet (mm), k_{sat} is the saturation factor, α_i is the ratio of pole face width to the pole pitch at average radius, D_{ro} and D_{ri} are the outer and inner diameter of rotor disc (mm), and p is the number of pole pairs.

C. Single phase equivalent circuit

The equation to identify the number of stator turn per phase (N_1) and the voltage induced by the rotor when it rotation (E_f) is given by [11]

$$N_1 = \frac{\varepsilon V_1}{\pi\sqrt{2} f k_{w1} \phi_f} \quad (3)$$

and

$$E_f = \sqrt{2} f N_1 k_{w1} \phi_f \quad (4)$$

where f is the frequency = 50 Hz, V_1 is the terminal voltage of generator (V), ε > 1 for generating mode, k_{w1} is the winding factor at fundamental harmonic.

Fig. 3 is the equivalent circuit of AFPMG. When the generator runs and connected to a load, the induced current (I_a) starts flowing in the stator winding, generates magnetomotive force and interacts with the main field produced by the rotor causing a change in direction and magnitude of the magnetic flux in the air gap. This is usually called an armature reaction. The armature reaction voltage lags the current by 90° and is presented by (-j$I_{ad}X_{sd}$) + (-j$I_{aq}X_{sq}$). The current I_{ad} produces maximum air gap field aligned with the rotor pole (d-axis), and I_{aq} aligned with the q-axis (between poles). The stator coil has resistance R_1 and leakage reactance X_1.

The value of R_1 is found with equation (5)

$$R_1 = \frac{N_1 l_{1av}}{a_p a_w \sigma s_a} \quad (5)$$

with l_{1av} is the average length of the stator turn (m), a_p is the number of the parallel current paths, a_w is the number of parallel conductors, σ is the electric conductivity of armature conductor (S/m), and S_a is the conductor cross section (m^2).

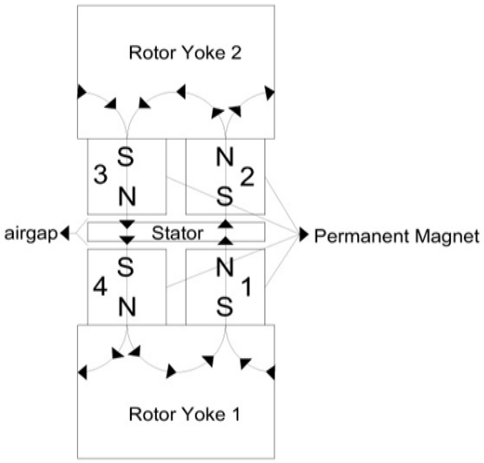

Figure 2. The geometry and magnetic flux path of double-sided rotors internal coreless stator AFPMG

Table 2.
The resistive and inductive load

Cos ϕ = 1		Cos ϕ = 0.85	
R_L(Ω)	X_L (Ω)	R_L(Ω)	X_L (Ω)
400	0	400	247.895
360	0	360	223.105
320	0	320	198.316
280	0	280	173.526
240	0	240	148.737
200	0	200	123.947
160	0	160	99.158
120	0	120	74.368
80	0	80	49.579
40	0	40	24.789
		30	18.592

The sum of the armature or mutual reactance X_a and X_1 yields synchronous reactance X_s, stated with

$$X_{sd} = X_{ad} + X_1 \quad (6)$$

$$X_{sq} = X_{aq} + X_1 \quad (7)$$

where d and q represent the d- and q-axis respectively.

For coreless stator, the leakage reactance is assumed close to 0, so that $X_{sd} \approx X_{ad}$, and $X_{sq} \approx X_{aq}$. Furthermore,

$$X_{ad} = 2m_1\mu_0 f(\frac{N_1 k_{w1}}{p})^2 \frac{(R_{ro}{}^2 - R_{ri}{}^2)}{g_d'} k_{fd} \quad (8)$$

$$X_{aq} = 2m_1\mu_0 f(\frac{N_1 k_{w1}}{p})^2 \frac{(R_{ro}{}^2 - R_{ri}{}^2)}{g_q'} k_{fq} \quad (9)$$

where m_1 is the phase number, μ_0 is the permeability of vacuum, g'_d and g'_q is the d- and q-axis equivalent air gap length respectively, k_{fd} and k_{fq} is the form factor in the d- and q-axis consecutively, with k_{fd} and k_{fq} equal to 1 for surface configuration of a permanent magnet.

The armature current is

$$I_a = I_{ad} + I_{aq} \quad (10)$$

If the generator is connected to an electrical load, then

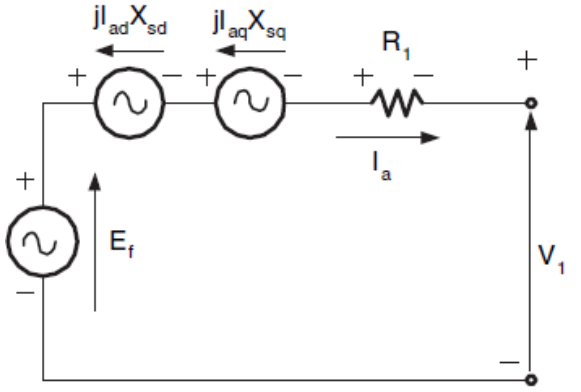

Figure 3.Single phase equivalent circuit of AFPMG [11]

$$I_{ad} = \frac{E_f(X_{sq} + X_L)}{(X_{sd} + X_L)(X_{sq} + X_L) + (R_1 + R_L)^2} \quad (11)$$

$$I_{aq} = \frac{E_f(R_1 + R_L)}{(X_{sd} + X_L)(X_{sq} + X_L) + (R_1 + R_L)^2} \quad (12)$$

where R_L and X_L are the load resistance and reactance in Ω consecutively.

D. Output power and voltage regulation

The terminal voltage (V_1) and output power (P_{out}) due to the load impedance (Z_L) are calculated with

$$V_1 = I_a Z_L \quad (13)$$

$$P_{out} = m_1 V_1 I_a \cos\phi \quad (14)$$

$$\phi = \arccos\left(\frac{I_a R_1}{V_1}\right) = \arccos\left(\frac{R_1}{Z_L}\right) \quad (15)$$

where Z_L is the load impedance and ϕ is the power factor angle.

The simulated loads R_L and X_L that give two different load power factor (PF) 1 and 0.85 are listed in Table 2. The percentage change in the output voltage from no-load (V_{nl}) to full-load (V_{fl}) when the generator is loaded by unity, lagging and leading power factor, or also called as voltage regulation VR is obtained using equation (16) [13],

$$VR = \frac{V_{nl} - V_{fl}}{V_{fl}} x\ 100\ \% \quad (16)$$

Generator losses including winding loss ΛP_1 (W), eddy current loss ΛP_e (W) and rotational loss ΔP_{rot} (W) are presented by,

$$\Lambda P_1 = m_1 I_a^2 R_1 \quad (17)$$

$$\Lambda P_e = \frac{\pi^2}{4}\frac{\sigma}{\rho} f^2 d^2 m_{con} [\, B_{mx1}^2 + B_{mz1}^2] \eta_d^2 \quad (18)$$

$$\Delta P_{rot} = \Delta P_{fr} + \Delta P_{wind} \quad (19)$$

where ρ is the specific mass density of the conductor (kg/m^3), m_{con} is mass of the stator conductor without end connection and insulation (kg), d is the diameter of the stator conductor (m), B_{mx1} and B_{mz1} are the peak values of tangential and axial components of the magnetic flux density (T) respectively, and η_d is the coefficient of distortion. For the last, the efficiency of the generator is expressed in equation (20)

$$\eta = \frac{P_{out}}{P_{out} + \Delta P} = \frac{P_{out}}{P_{out} + (\Delta P_1 + \Delta P_e + \Delta P_{rot})} \quad (20)$$

III. Results and Discussions

A. Magnetic field distribution

The magnetic field distributions of the generator in no-load and on loaded conditions are shown in Fig. 4. For the simulation, the load current correlated with the PF=1 is 5.57 A and for the PF = 0.85 is 6.32 A.

At no-load condition (Fig. 4a), the magnetic flux is only produced by permanent magnets on the rotor. The maximum value of flux density $|B|$ (in the box) is the highest (1.049 T) compared to the underloaded condition. When load R_L and $R_L + jX_L$ are applied, the magnetic flux generated by the current flowing in the conductors suppresses the magnetic flux produced by the magnets, which results in a decrease in the maximum $|B|$. Both simulated loads give the same maximum values of $|B|$, which is 1.047 T (Fig. 4b & c). In general, all the results in Fig. 4 exhibits good magnetic flux distribution on the stator and rotor indicated by the absence of the flux concentration spots. Besides, all the maximum flux densities are lower than the saturation point 2.2 T.

As previously explained, the armature reaction takes place in the air gap. From Figure 5, it can be seen the inverse correlation between the air gap flux density B_{mg} and the load current. The peaks of B_{mg} waves can be observed clearly between the no-load and loaded condition but it appears to coincide between the loaded ones due to a very small difference in value. The peak values of each wave are 0.80896 T, 0.7731 T and 0.76785 T for no-load, PF = 1 and PF = 0.85 consecutively.

B. Generator performance prediction

The calculation results of I_a, V_1, P_{out}, VR and η, at load R_L and $R_L + jX_L$ are presented in Table 3 and Table 4. For easy comparison, the parameters in Table 3 and Table 4 are graphically illustrated as shown in Fig. 6 to Fig 9. In a synchronous generator using a stator core of any size, the winding resistance is frequently neglected because its value is considered too small compared to the synchronous reactance. However, it is different from a coreless generator. From the calculation, it is obtained X_{sq} = 0.036 Ω and R_1 = 2.39 Ω, or in other words, the internal load is more resistive. With two types of the given loads, I_a is higher when the load is R_L and this causes a higher internal voltage drop, which finally results in lower V_1

Table 3.
Calculation results of the electrical parameters at load R_L

R_L (Ω)	I_a (A)	V_1 (V)	P_{out} (W)	VR (%)	η (%)
400 < 0°	0.59	236.16	137.78	0.60	74.26
360 < 0°	0.65	234.76	152.88	0.66	76.13
320 < 0°	0.73	234.60	171.71	0.75	78.08
280 < 0°	0.84	234.41	195.82	0.85	80.12
240 < 0°	0.97	234.16	227.82	1.00	82.24
200 < 0°	1.17	233.83	272.31	1.19	84.44
160 < 0°	1.45	233.37	338.39	1.49	86.69
120 < 0°	1.93	232.68	446.79	1.99	88.89
80 < 0°	2.87	231.55	657.29	2.99	90.81
40 < 0°	5.57	229.31	1241.53	5.97	91.11

Table 4.
Calculation results of the electrical parameters at load Z_L

Z_L (Ω)	I_a (A)	V_1 (V)	P_{out} (W)	VR (%)	η (%)
400 < 31.79°	0.50	236.16	99.86	0.44	67.76
360 < 31.79°	0.55	235.13	110.85	0.48	69.93
320 < 31.79°	0.62	235.02	124.56	0.55	72.25
280 < 31.79°	0.71	234.88	142.13	0.62	74.70
240 < 31.79°	0.83	234.70	165.48	0.73	77.31
200 < 31.79°	0.99	234.45	198.00	0.87	80.07
160 < 31.79°	1.24	234.12	246.43	1.09	82.96
120 < 31.79°	1.65	233.61	326.22	1.46	85.93
80 < 31.79°	2.46	232.77	482.36	2.19	88.72
40 < 31.79°	4.81	231.11	924.45	4.39	90.05
30 < 31.79°	6.32	226.23	1198.47	5.86	89.38

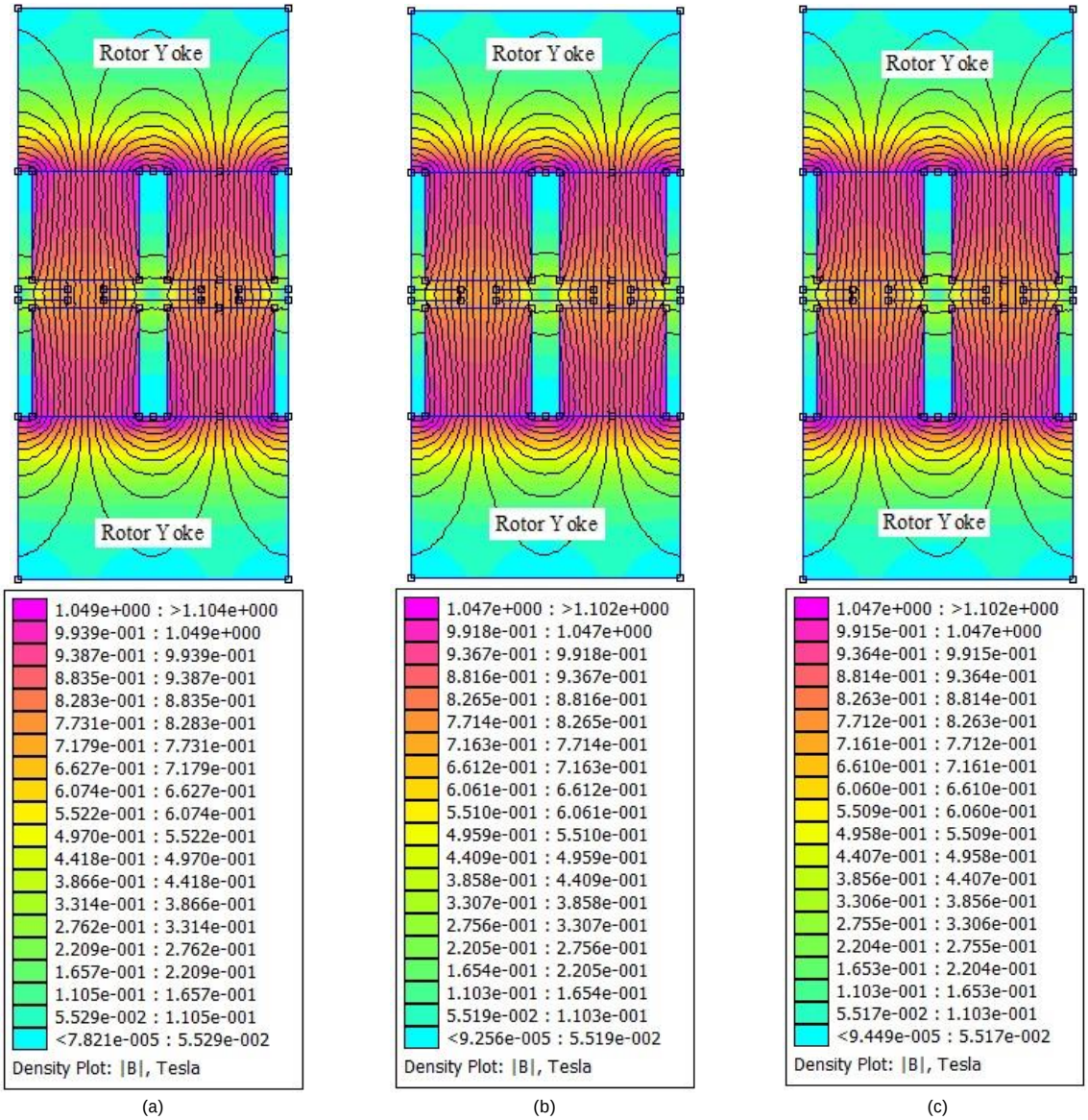

Figure 4. Magnetic field distributions under; (a) no-load condition; (b) load R_L; (c) load $R_L + jX_L$

(Fig. 6). For having better power factor, the generator with load R_L produces better output power (Fig. 7) and its efficiency is also slightly higher accordingly (Fig. 8), with the best value of 91.11 % at 5.57 A. Generator with load Z_L provides the highest efficiency of 90 % at 4.81 A and then it goes down for saturation.

According to Eq. (16), *VR* represents the ratio of voltage drop (from no load to full load) to the no-load voltage. Therefore, it should be as low as possible to gain a stable power distribution. It is already mentioned that a higher voltage drop occurs when the load is R_L (with referring to Fig. 6). Consequently,

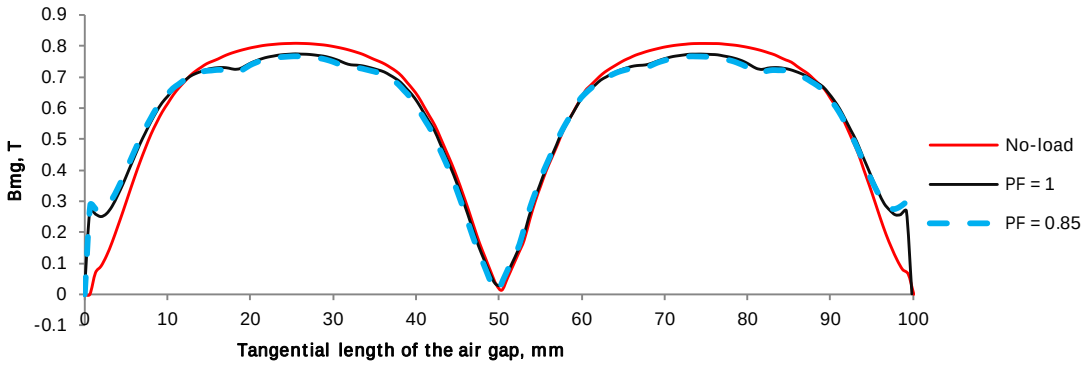

Figure 5. Magnetic flux density

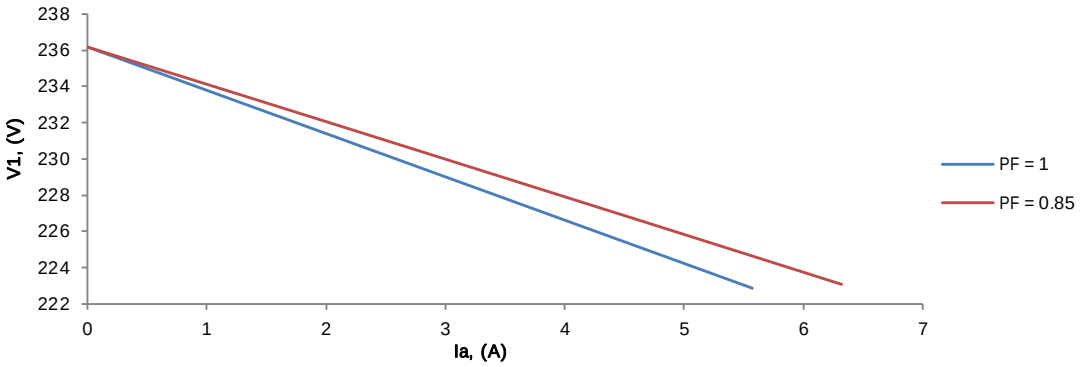

Figure 6. V_1 vs I_a

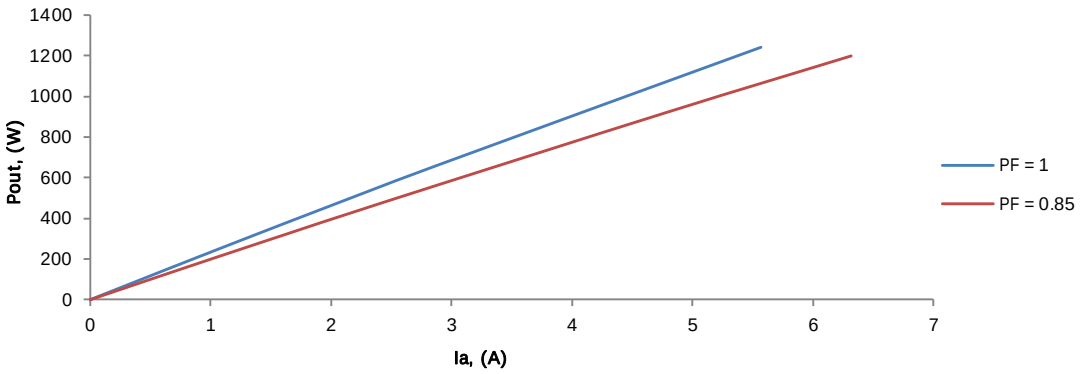

Figure 7. P_{out} vs I_a

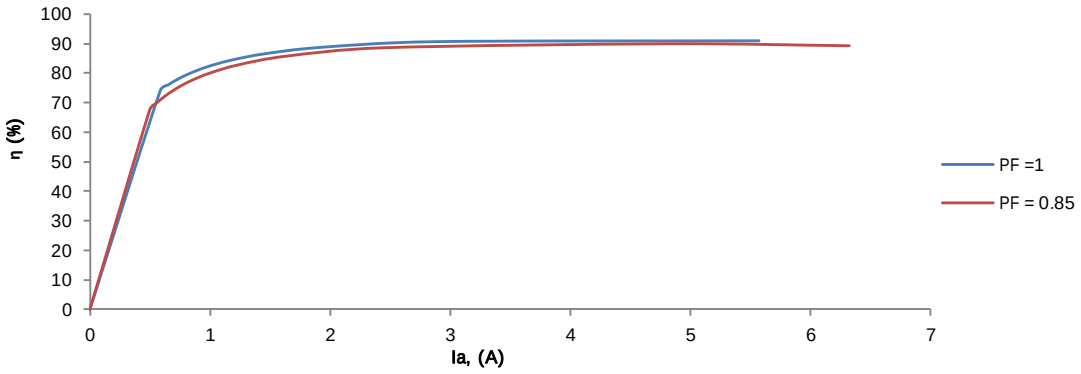

Figure 8. η vs I_a

the *VR* is also higher with the maximum value of 5.97 %, and for PF = 0.85 or load Z_L, *VR* = 5.86 % (Fig. 9). These values meet the requirement, which is below 8 %, according to IEC 60364: Low voltage electrical installation, part 5-52: Selection and erection of electrical equipment - wiring Systems.

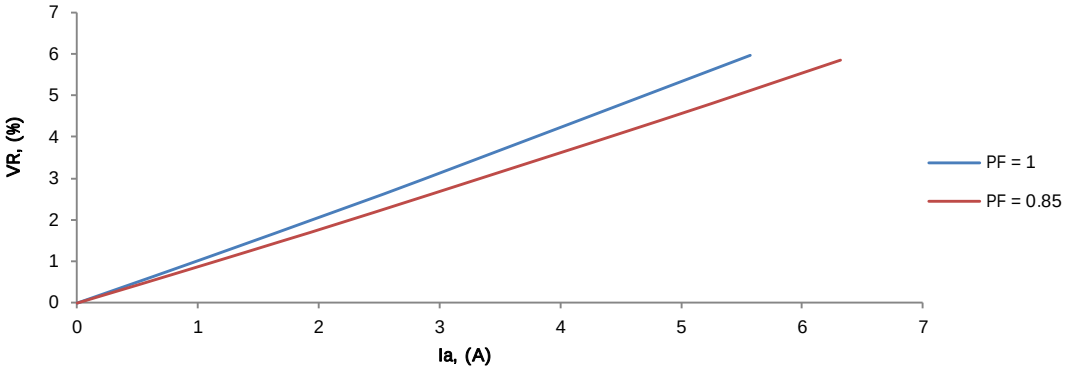

Figure 9. VR vs I_a

IV. Conclusion

Load characteristic analysis of the double-side internal coreless stator AFPMG has been discussed in this paper. The applied load is resistive and resistive-inductive in series, which gives the power factor of 1 and 0.85 respectively. From the simulation, it is found that when loaded with resistive load, the coreless generator delivers higher armature current but this gives a consequent in higher voltage drop indicated by lower terminal voltage and higher voltage regulation. Nevertheless, with a better power factor, the output power and efficiency are higher. It is opposite to the generator that is loaded with impedance. According to the results, it can be concluded that the coreless generator performance is superior in the output power (1,241 W) and efficiency (91 %) with resistive load; on the other hand, the voltage regulation is better (5.86 %) with impedance load. From each parameter being compared, the difference in values is relatively small, so in principle, the generator provides good performance in both loads.

Acknowledgement

The authors would like to thank all the facilities provided by the Indonesian Institute of Sciences (LIPI), particularly to the Research Center for Electrical Power and Mechatronics during the process of making this manuscript.

Declarations

Author contribution

K. Wirtayasa and P. Irasari contributed equally as the main contributor of this paper. All authors read and approved the final paper.

Funding statement

This research did not receive any specific grant from funding agencies in the public, commercial, or not-for-profit sectors.

Conflict of interest

The authors declare no conflict of interest.

Additional information

No additional information is available for this paper.

References

[1] S. S. Soe and Y. A. Oo, "Design of the Coreless Axial-Flux Double-Sided Permanent Magnet Synchronous Generator for Wind Power System," *Int. J. Sci. Eng. Technol. Res.*, vol. 3, no. 10, pp. 2047–2051, 2014.

[2] S. Saint Soe and Y. A. N. A. Oo, "Design and Implementation of the Double-Sided Axial-Flux PMSG with Slotted Stator by Using Sizing Equation and FEA Software," in *Proceedings of Nineteenth TheIIER International Conference,* 2015, no. April, pp. 63–69.

[3] D. Ahmed and A. Ahmad, "An optimal design of coreless direct-drive axial flux permanent magnet generator for wind turbine," *J. Phys. Conf. Ser.*, vol. 439, 2013.

[4] A. Daghigh, H. Javadi, and H. Torkaman, "Improved design of coreless axial flux permanent magnet synchronous generator with low active material cost," in *The 6th International Power Electronics Drive Systems and Technologies Conference (PEDSTC2015)*, 2015, pp. 532–537.

[5] S. S. Bageshwar, P. V Phand, R. V Phand, P. G. Student, and U. G. Student, "Design & Analysis of Axial Flux Permanent Magnet Synchronous Generator," *Int. J. Res. Trends Innov.*, vol. 2, no. 7, pp. 123–129, 2017.

[6] M. Chirca, S. Breban, C. A. Oprea, and M. M. Radulescu, "Analysis of Innovative Design Variations for Permanent-Magnet Generators in Micro-Wind Power Applications," in *2014 International Conference on Electrical Machines (ICEM)*, 2014, pp. 385–389.

[7] A. O. Otuoze, O. O. Ogidi, O. O. Mohammed, A. A. Jimoh, and B. S. Olaiya, "Sizing of Wind Powered Axial Flux Permanent Magnet Alternator Using Analytical Approach," *Niger. J. Technol.*, vol. 35, no. 4, pp. 919–925, 2016.

[8] M. R. Minaz and M. Çelebi, "Design and analysis of a new axial flux coreless PMSG with three rotors and double stators," *Results Phys.*, vol. 7, pp. 183–188, 2017.

[9] M. R. Minaz and M. Çelebi, "Analysis and Design of an Axial-Flux Coreless Permanent Magnet Synchronous Generator with Single Stators and Double Rotors," *Int. J. Energy Appl. Technol.*, vol. 4, no. 1, pp. 7–11, 2017.

[10] D. Chung and Y. You, "Design and Performance Analysis of Coreless Axial-Flux Permanent-Magnet Generator for Small Wind Turbines," *J. Magn.*, vol. 19, no. 3, pp. 273–281, 2014.

[11] J. F. Gieras, R. Wang, and M. J. Kamper, "Axial Flux Permanent Magnet Brushless Machines", 2nd ed. Springer, 2008.

[12] S. Kim, J. Li, D. Choi, and Y. Cho, "Design and analysis of Axial Flux Permanent Magnet Generator for Direct-Driven Wind Turbines," *Int. J. Power Syst.*, vol. 2, pp. 1–6, 2017.

[13] T. S. El-hasan, "Development of Automotive Permanent Magnet Alternator with Fully Controlled AC / DC Converter," *Energies*, vol. 11, no. 274, pp. 1–28, 2018.